Effect of energy loss on the lateral spread of MeV helium ions in C, Al, and Cu: Comparison with experimental data

A. Mekhtiche
Laboratoire PTEAM, Faculté des Sciences, Université Dr Yahia Fares, Pôle urbain, Médéa, Algeria.

K. Khalal-Kouache
Laboratoire SNIRM, Faculté de Physique, Université des Sciences et de la Technologie Houari Boumediene (USTHB), Algiers, Algeria.

Received 8 October 2025; accepted 23 March 2026

The Marwick-Sigmund model has been widely used to calculate the lateral spread of ions transmitted through matter. However, this model neglects the effect of ion energy loss within the target material. In this study, the model was employed to calculate the lateral spread distributions of MeV helium ions transmitted through carbon, aluminum, and copper targets. Ion energy loss was incorporated into the calculations using an approach analogous to that used for determining the angular distributions of transmitted ions. A comparison of our results with experimental data indicates that incorporating energy loss substantially enhances the overall agreement. Furthermore, this approach provides a rigorous method to account for lateral spread in depth resolution estimates for ion-beam analysis, particularly when nuclear stopping is a significant component of total stopping power.

Keywords: Lateral spread; multiple scattering; transport theory; interaction potential; energy loss; depth-resolution.

DOI: https://doi.org/10.31349/RevMexFis.72.050401

1. Introduction

The study of ion-matter interactions constitutes a fundamental research area in many fields, including semiconductor device fabrication [1], nanotechnology [2], and radiation applications [3]. It involves processes such as ion energy loss and ion range, which govern particle transport and material modification. Therefore, a deep understanding of these processes is essential for the development of models that describe ion behavior in various media.

When an ion beam traverses matter, it undergoes electronic and nuclear interactions with target atoms, resulting in energy loss and angular deviation. The successive deflections due to the interactions with target atoms, known as multiple scattering, result in angular and lateral distributions of the ion beam. While lateral spread broadens the beam and introduces path-length fluctuations [4], understanding this phenomenon is crucial in various practical fields, including proton therapy [5], ion-beam imaging [6], external microbeam analysis of lithium batteries [7], high-resolution in-air ion-beam applications [8], nanofabrication [9, 10], and depth profiling [11]. In these domains, lateral spread imposes fundamental limits on achievable spatial resolution and introduces path-length fluctuations that directly contribute to the uncertainty of depth and energy measurements. For instance, in ion-beam analysis techniques such as RBS (Rutherford Backscattering Spectrometry) and ERDA (Elastic Recoil Detection Analysis), the lateral component of multiple scattering contributes to the energy spread of detected particles, thereby degrading depth resolution, particularly at large penetration depths. Accurate quantification of this contribution, therefore, remains essential for interpreting and optimizing ion-beam experiments.

Although the theoretical foundations of the multiple scattering of charged particles in random media were established in early analytical works [12–15] and later reformulated [16–18], this theory continues to serve as a standard framework for interpreting experimental data on particle transport in matter [19–22]. Amsel *et al.* [23] provided a comprehensive review of the theory and its typical applications. Sigmund and Winterbon (SW) [17] and Marwick and Sigmund (MS) [18] developed two multiple scattering models to calculate the angular distribution and lateral spread of transmitted particles, respectively. These models, derived from transport theory, were formulated under the assumptions of a random medium, binary collisions with small scattering angles, and negligible energy loss. Subsequently, the SW model was generalized by Valdés and Arista (VA) [24] to incorporate energy loss into the angular distribution calculations. In contrast, incorporating energy loss into lateral spread calculations remains challenging, despite earlier attempts using the power-law potential [25]. In ion-beam analysis applications, the layered numerical formalism introduced by Szilágyi *et al.* [26] provides a computationally efficient framework for integrating continuous slowing-down effects into lateral-dispersion calculations. Serving as the computational kernel for the DEPTH code [26] and implemented in standard software such as SIMNRA [27] and WiNDF [28], this formalism is essential for evaluating depth resolution and path-length fluctuations in RBS and ERDA measurements. However, comparisons with Monte Carlo and molecular dynamics simulations indicated that this analytical approach exhibits systematic deviations at significant depths, attributed in part to the neglect of nuclear stopping power [29]. Moreover, Androulakaki *et al.* [30] have recently noted that applying this framework to the large penetration depths investigated in their study required extrapolating the theory beyond its original design limits.

Experimentally, angular distributions are evaluated using solid targets, whereas lateral spread measurements are commonly performed using gas targets. However, experimental data on the lateral spread in solid materials have been reported in only one study [31]. In that study, several carbon, aluminum, and copper targets were employed, and lateral spread measurements were performed using RBS or nuclear reaction techniques. Notably, this is one of the few studies that examine the lateral spread under conditions involving significant ion energy loss.

The present study represents a continuation of our comprehensive investigation into the effects of energy loss on ion multiple scattering [32–35]. Specifically, we analyze the lateral spread of helium ions transmitted through carbon, aluminum, and copper targets using the MS model, which we modified to account for ion energy loss in a manner analogous to the VA model's treatment of angular distributions. The main contribution is a comparison of calculated lateral-spread widths, as functions of penetration depth and ion energy, with the experimental data from Ref. [31].

2. Lateral spread theory

We consider a collimated beam of monoenergetic charged particles transmitted along the positive x-direction of an amorphous foil of thickness x (Fig. 1). The lateral distribution $G(x,\rho)$ of transmitted particles is given by [18]:

$$G(x,\rho)\,\mathrm{d}^2\rho = \frac{\rho}{x}\,\mathrm{d}\left(\frac{\rho}{x}\right)\int_0^\infty k\,\mathrm{d}k\,J_0\left(\frac{k\rho}{x}\right) \times \exp\left[-\frac{Nx}{k}\int_0^k \sigma_0(k',E)\,\mathrm{d}k'\right], \quad (1)$$

where $\rho = \sqrt{\rho_y^2+\rho_z^2}$ is the lateral displacement. J_0 is the zero-order Bessel function of the first kind, N is the number of scattering centers per unit volume, E is the initial energy of the incident ion, and $\sigma_0(k',E)$, the transport cross section, is given by:

$$\sigma_0(k',E) = \int_0^\infty d\sigma(\phi)\,[1-J_0(k'\phi)], \quad (2)$$

where ϕ is the single scattering angle defined in the laboratory frame and $d\sigma(\phi)$ is the differential cross section.

By introducing the reduced variables τ and $\tilde{\rho}$, which are defined in terms of the thickness x and the lateral displacement ρ as follows:

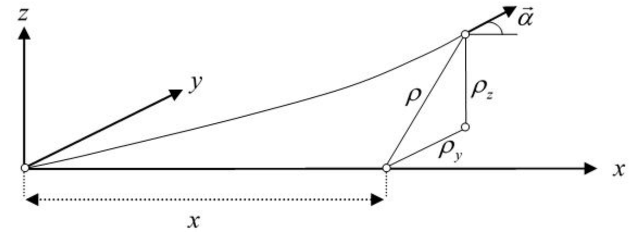

FIGURE 1. Geometry under consideration: The initial beam direction coincides with the positive x-axis. A lateral displacement ρ and an angular deviation $\vec{\alpha}$ are considered after a penetration depth x.

$$\tau = \pi a^2 N x, \quad (3)$$

$$\tilde{\rho} = \pi a^2 N\,\frac{E\,a}{2Z_1Z_2e^2}\rho, \quad (4)$$

where a is the screening radius, and Z_1 and Z_2 are the atomic numbers of the ion and the target atom, respectively. The function $G(x,\rho)$ can be represented in terms of the reduced lateral distribution function $g_1(\tau,\tilde{\rho})$ as follows:

$$G(x,\rho)\,d^2\rho = g_1(\tau,\tilde{\rho})\,\tilde{\rho}\,d\tilde{\rho}, \quad (5)$$

with

$$g_1(\tau,\tilde{\rho}) = \frac{1}{\tau^2}\int_0^\infty z\,dz\,J_0\left(z\frac{\tilde{\rho}}{\tau}\right) \times \exp\left[-\frac{\tau}{z}\int_0^z d\gamma\,\Delta(\gamma)\right]. \quad (6)$$

The function $\Delta(\gamma)$, called the reduced transport cross section, is given by:

$$\Delta(\gamma) = \int_0^\infty \frac{d\tilde{\phi}}{\tilde{\phi}^2}\,f(\tilde{\phi})\left[1-J_0(\gamma\tilde{\phi})\right], \quad (7)$$

where $\tilde{\phi}$ is the reduced single scattering angle, and f is the scattering function determined by the interaction potential.

In the original MS model of lateral spread, ion energy loss was neglected during its entire trajectory within the target. This implies that the cross section $\sigma_0(k',E)$, defined by Eq. (2), is calculated at a fixed energy E corresponding to the ion's initial energy. For thin targets, which are related to low ion energy loss, this approximation is justified. However, as the target thickness increases and energy loss becomes significant, the assumption of negligible energy loss is no longer valid. In such cases, a more rigorous analysis is essential to consider the cross section at every possible instantaneous energy $E\,(x')$, corresponding to any path x' traversed by the ion inside the medium. To incorporate this, we apply the following substitution, previously introduced in the VA model [24], to Eq. (1):

$$x\,\sigma_0(k,E) \to \int_0^x \sigma_0\left(k,E(x')\right)dx', \quad (8)$$

or in terms of reduced quantities:

$$\tau\,\Delta(\gamma) \to \int_0^\tau \Delta(\gamma')d\tau'. \quad (9)$$

The new reduced transport cross section $\Delta(\gamma')$ is now expressed as:

$$\Delta(\gamma') = \int_0^\infty \frac{d\tilde{\phi}}{\tilde{\phi}^2} f(\tilde{\phi}) \left[1 - J_0(\gamma'\tilde{\phi})\right], \qquad (10)$$

with:

$$\gamma' = \frac{\mathrm{E}}{\mathrm{E}(x')}\gamma. \qquad (11)$$

The instantaneous energy $E(x')$ is expressed as:

$$E(x') = E - \int_0^{x'} \left(\frac{dE}{dx}\right) dx. \qquad (12)$$

Here dE/dx is the total stopping power (electronic and nuclear).

It is important to note that the substitution given by Eq. (8) is valid under the condition that, for a given foil thickness x, the ion's path length L is considered equivalent to the foil thickness x. This approximation should be validated at high energy loss, where increased angular straggling can increase L/x.

3. Results and discussion

To verify that the ion path length L remains close to the foil thickness x, Monte Carlo simulations were performed using TRIM (SRIM 2013) [36] for 1-2 MeV ^{4}He ions and 1 MeV ^{3}He ions transmitted through carbon, aluminum, and copper targets. In the experimental systems of Möller and Williams [31], the largest relative energy loss values ($\Delta E/E$), where ΔE is the projectile's total energy loss in the target, were approximately 0.36 for ^{4}He in C, 0.22 for ^{4}He in Al, and 0.48 for ^{3}He in Cu. To test the validity of the approximation $L \approx x$ under conditions at least as severe as those in the experiments, we simulated target thicknesses corresponding to $\Delta E/E = 0.50$, slightly exceeding the maximum experimental value (0.48) reported in Ref. [31]. Figure 2 shows representative path-length distributions as a function of L/x, demonstrating that the vast majority of ions are transmitted with path lengths very close to x. These results support the validity of the $L \approx x$ approximation adopted in this study. Regarding the projectile charge state, the experimental study in Ref. [31] employed MeV $^3\mathrm{He}^+$ and $^4\mathrm{He}^+$ beams. However, the initial vacuum charge state need not be specified in the present treatment. MeV helium reaches charge equilibrium within a few to tens of nanometers [37, 38], a depth far smaller than the $0.3 - 20\ \mu\mathrm{m}$ targets used by Möller and Williams [31] . Ion spread is therefore governed by near-equilibrium charge states, in which helium projectiles behave effectively as nearly fully stripped He^{2+} ions [38, 39].

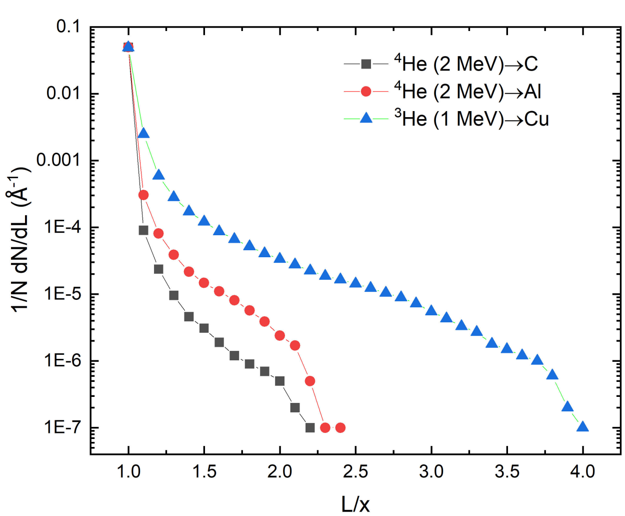

FIGURE 2. Path-length distribution as a function of L/x for He ions transmitted through C and Al films at 2 MeV (squares and circles, respectively), and through a Cu film at 1 MeV (triangles). The considered target thicknesses correspond to a relative energy loss $\Delta E/E = 0.5$.

Using the MS model, the lateral distributions of helium ions with energies of 1 and 2 MeV transmitted through C, Al, and Cu targets were calculated. The projectile instantaneous energy $E(x')$ was computed numerically from Eq. (12) using the total stopping power (electronic and nuclear) obtained from the SRIM compilation [36]. The resulting $E(x')$ was fitted and substituted into Eq. (11) to calculate γ'. The lateral distribution $G(x,\rho)$ (Eq. (1)), or equivalently the reduced distribution $g_1(\tau,\tilde{\rho})$ (Eq. (6)), was computed using the reduced transport cross section $\Delta(\gamma)$ from Eq. (7) when energy loss is neglected, or $\Delta(\gamma')$ from Eq. (10) when energy loss is included. In all cases, the Thomas-Fermi-MoliÃ¨re (TFM) potential [40] was used to describe the interaction between He ions and the various targets. An example of these calculations is presented in Fig. 3, illustrating the case of 1 MeV ^3He ions transmitted through a Cu target of thickness x= 700 $\mu\mathrm{g/cm}^2$. The areal thickness of the target (in $\mu\mathrm{g/cm}^2$ units) was chosen to match the metric used in the experimental results of Ref. [31]. It can be observed that including energy loss affects the shape of the distribution, resulting in a

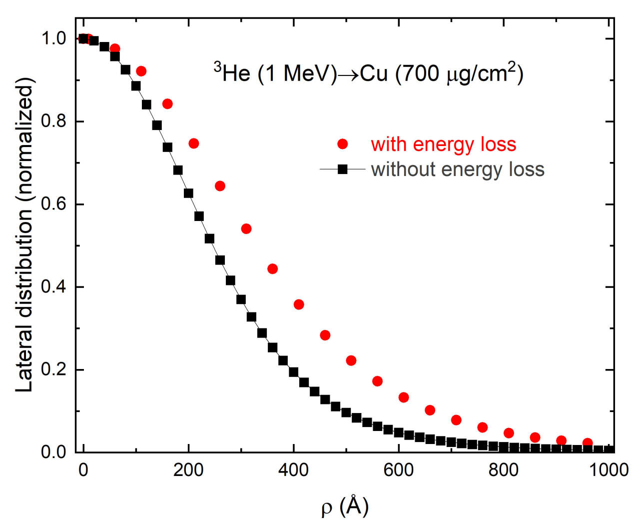

FIGURE 3. Lateral distributions of 1 MeV ^{3}He ions transmitted through a Cu target of $x = 700\ \mu\mathrm{g/cm}^2$ thickness.

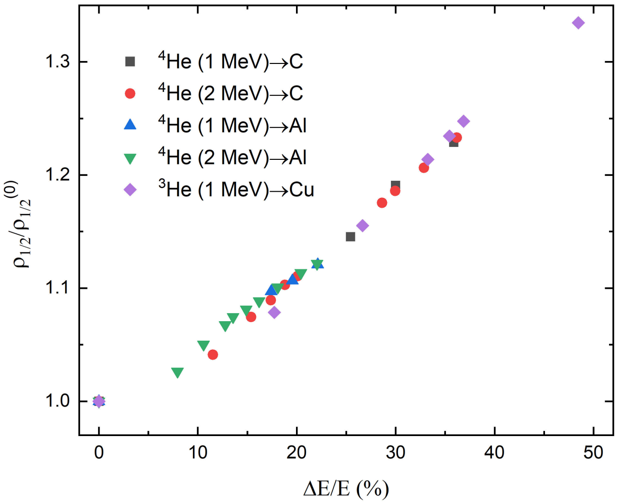

FIGURE 4. Variation of the ratio $\rho_{1/2}/\rho_{1/2}^{(0)}$ with the relative ion energy loss for different targets.

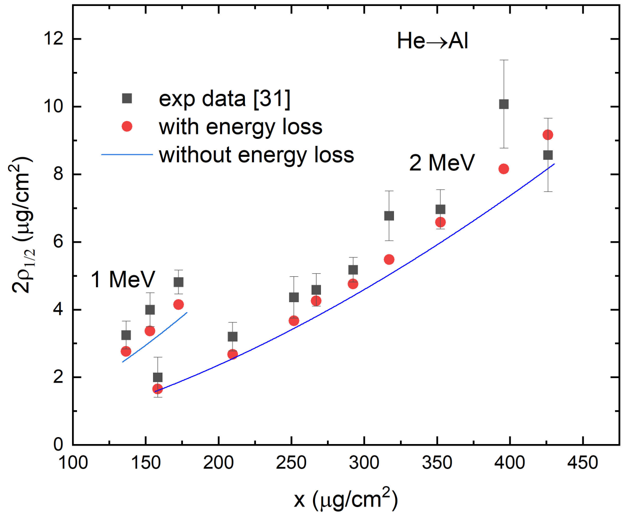

FIGURE 6. Same as Fig. 5 but for ^4He ions transmitted through an Al target.

broader profile. These results are consistent with those obtained when energy loss is taken into account in the angular distribution calculations [24, 33]. It is worth noting that the relative ion energy loss $\Delta E/E$ in this case is approximately 50%.

For comparison with the experiment, the half-width $\rho_{1/2}$, defined as the lateral displacement at which the distribution reaches half of its maximum value, was extracted from each calculated lateral distribution. It is defined by the condition:

$$G(x, \rho_{1/2}) = 0.5\, G(x, 0). \tag{13}$$

After normalizing each distribution at zero lateral displacement, $\rho_{1/2}$ was determined numerically by interpolating the distribution near the half-maximum and extracting the corresponding lateral displacement. The symbols $\rho_{1/2}^{(0)}$ and $\rho_{1/2}$

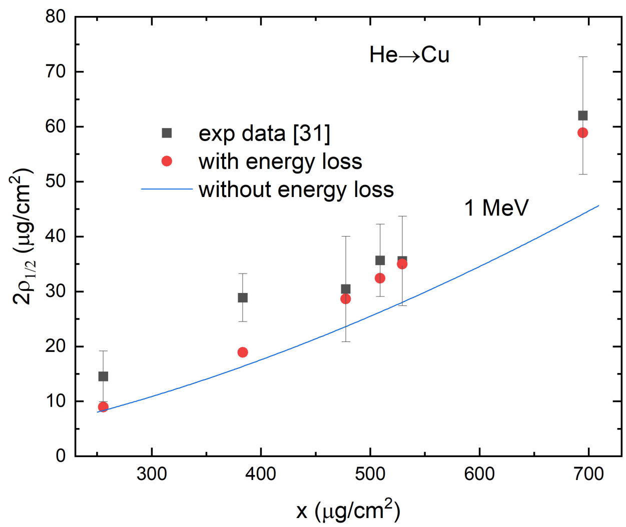

FIGURE 7. Same as Fig. 5 but for ^3He ions transmitted through a Cu target.

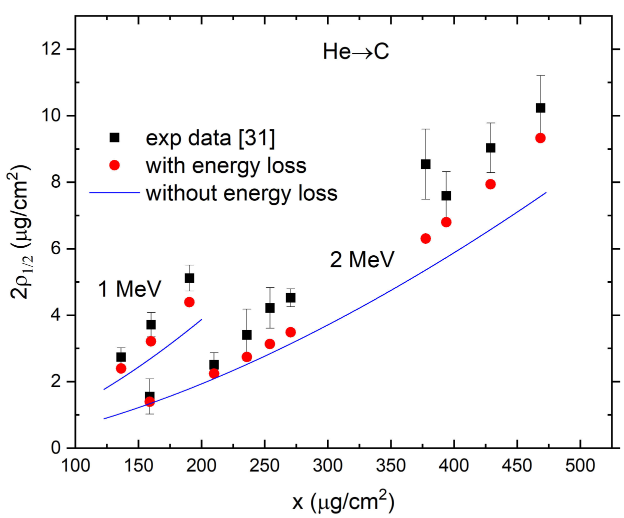

FIGURE 5. Variation of $2\rho_{1/2}$ as a function of target thickness x for ^4He ions transmitted through a C target. Squares: experimental data from [31]; solid lines: calculations without considering energy loss; circles: calculations including energy loss.

denote the values obtained without and with energy loss included, respectively. The half-widths, initially expressed in Å, were converted to $\mu\text{g}/\text{cm}^2$ using the corresponding target mass densities. Figure 4 shows the variation of the ratio $\rho_{1/2}/\rho_{1/2}^{(0)}$ with the relative ion energy loss. The results indicate that this ratio, which exhibits a uniform shape, increases with the energy loss. It appears to be almost independent of both the projectile energy and target material within the considered range of energy loss. A similar behavior was observed in the ratio of the half-maximum values of the angular distributions obtained with and without accounting for energy loss in the calculations [33].

Figures 5, 6 and 7 show a comparison between the calculated values of $2\rho_{1/2}$ (in $\mu\text{g}/\text{cm}^2$ units) as a function of target thickness, obtained with energy loss taken into account, and the experimental data from Ref. [31]. The results are presented for the following cases: ^{4}He ions with energies of 1 and 2 MeV on C and Al targets, and ^{3}He ions with 1 MeV energy on a Cu target, respectively. The corresponding calculated values obtained without considering energy loss are also included in the figures.

These figures clearly demonstrate that incorporating energy loss into the calculations significantly improves agreement with the experimental data across the entire range of target thicknesses. In contrast, calculations that neglect energy loss yield reasonable agreement only at small thicknesses, where the relative energy loss is low. However, as the

target thickness increases and the energy loss becomes more pronounced, deviations between these calculations and the experimental results become more significant. Incorporating energy loss into the calculations significantly improves model accuracy across all target materials. The maximum discrepancy between experimental and calculated values decreases from 26% to 9% for carbon, from 28% to 19% for aluminum, and from 29% to 5% for copper targets. Thus, beyond the qualitatively expected increase in lateral spread, explicitly treating energy loss yields quantitative improvements in predictive accuracy, particularly at large $\Delta E/E$. The present results demonstrate the importance of considering stopping effects in lateral-spread calculations, particularly for ions traversing substantial depths in matter. The proposed method enables depth-resolution evaluations in ion-beam analysis, particularly when nuclear stopping constitutes a non-negligible fraction of the total stopping power, an effect not captured by the transformation approach of Szilágyi *et al.* [26].

4. Conclusions

In this study, a model based on transport theory was employed to calculate the lateral distributions of MeV He ions transmitted through carbon, aluminum, and copper targets. The assumption that the ion path length is equivalent to the foil thickness was rigorously tested using the TRIM code under conditions of high ion energy loss, demonstrating its applicability across all systems examined in this study. The effects of ion energy loss were added to the calculations using the VA model. The results show that when energy loss is taken into account, the calculated profiles change noticeably, becoming wider overall. Moreover, comparing the calculated half-widths of the lateral spread with experimental measurements highlights that including energy loss leads to much better agreement throughout the range of energy losses studied. This study emphasizes the necessity of incorporating energy loss into such calculations. Therefore, we recommend applying this method into future depth-resolution analyses, particularly in regimes where nuclear stopping cannot be neglected.

---

1. P. Kumar, M. I. M. Martins, M. E. Bathen, T. Prokscha, U. Grossner, Al-implantation induced damage in 4H-SiC, *Mater. Sci. Semicond. Process.* **174** (2024) 108241, https://doi.org/10.1016/j.mssp.2024.108241
2. X. Zhang, K. Hattar, Y. Chen, L. Shao, J. Li, C. Sun, K. Yu, N. Li, M. L. Taheri, H. Wang, J. Wang, M. Nastasi, Radiation damage in nanostructured materials, *Prog. Mater. Sci.* **96** (2018) 217, https://doi.org/10.1016/j.pmatsci.2018.03.002
3. A. Herklotz, T. Z. Ward, S. Zhou, Modulating oxide-based quantum materials by ion implantation, *Adv. Funct. Mater.* **35** (2025) 2506647, https://doi.org/10.1002/adfm.202506647
4. G. Mao, J. Guo, W. Liu, Study on the lateral scattering of high-energy heavy ions penetrating through solids, *Phys. Status Solidi A* **220** (2023) 2200515, https://doi.org/10.1002/pssa.202200515
5. R. Mohan, A review of proton therapy – current status and future directions, *Precis. Radiat. Oncol.* **6** (2022) 164, https://doi.org/10.1002/pro6.1149
6. E. Vittone, Semiconductor characterization by scanning ion beam induced charge (IBIC) microscopy, *ISRN Condens. Matter Phys.* **2013** (2013) 637608, https://doi.org/10.1155/2013/637608
7. T. Tadić, M. Jakšić, C. Capiglia, Y. Saito, P. Mustarelli, External microbeam PIGE study of Li and F distribution in PVdF/HFP electrolyte gel polymer for lithium battery application, *Nucl. Instrum. Methods Phys. Res. B* **161–163** (2000) 614, https://doi.org/10.1016/S0168-583X(99)00849-6
8. M. Jakšić, D. Chokheli, S. Fazinić, V. Grilj, N. Skukan, I. Sudić, T. Tadić, T. Antičić, In-air ion beam analysis with high spatial resolution proton microbeam, *Nucl. Instrum. Methods Phys. Res. B* **371** (2016) 185, https://doi.org/10.1016/j.nimb.2015.11.012
9. S. Mo, D. O. Byrne, F. I. Allen, Focused helium ion beam nanofabrication by near-surface swelling, *J. Vac. Sci. Technol. B* **43** (2025) 022803, https://doi.org/10.1116/6.0004100
10. R. O'Meara, V. Dhyani, B. R. Tak, A. McClelland, G. Dawson, C. Storey, A. P. G. Robinson, B. Holst, R. G. Hobbs, Measurement of the lithographic point-spread function of a focused helium ion beam in negative-tone PMMA and fullerene resists on ultrathin membranes, *Microelectron. Eng.* **302** (2026) 112405, https://doi.org/10.1016/j.mee.2025.112405
11. S. Möller, H. Joo, M. Rasinski, M. Mann, E. Figgemeier, M. Finsterbusch, Quantitative lithiation depth profiling in silicon containing anodes investigated by ion beam analysis, *Batteries* **8** (2022) 14, https://doi.org/10.3390/batteries8020014
12. W. Bothe, Das allgemeine Fehlergesetz, die Schwankungen der Feldstärke in einem Dielektrikum und die Zerstreuung der α-Strahlen, *Z. Phys.* **5** (1921) 63, https://link.springer.com/article/10.1007/BF01349687

13. E. J. Williams, Concerning the scattering of fast electrons and of cosmic-ray particles, *Proc. R. Soc. A* **169** (1939) 531, https://doi.org/10.1098/rspa.1939.0015

14. S. Goudsmit, J. L. Saunderson, Multiple scattering of electrons, *Phys. Rev.* **57** (1940) 24; **58** (1940) 36, https://doi.org/10.1103/PhysRev.57.24

15. H. S. Snyder, W. T. Scott, Multiple scattering of fast charged particles, *Phys. Rev.* **76** (1949) 220, https://doi.org/10.1103/PhysRev.76.220

16. L. Meyer, Plural and multiple scattering of low-energy heavy particles in solids, *Phys. Status Solidi B* **44** (1971) 253, https://doi.org/10.1002/pssb.2220440127

17. P. Sigmund, K. B. Winterbon, Small-angle multiple scattering of ions in the screened Coulomb region, *Nucl. Instrum. Methods* **119** (1974) 541, https://doi.org/10.1016/0029-554X(74)90805-2

18. A. D. Marwick, P. Sigmund, Small-angle multiple scattering of ions in the screened Coulomb region: 2. Lateral spread, *Nucl. Instrum. Methods* **126** (1975) 317, https://doi.org/10.1016/0029-554X(75)90693-X

19. M. Famá, G. H. Lantschner, J. C. Eckardt, Energy-angle distribution of low-energy hydrogen ions in thin aluminum and gold foils, *Nucl. Instrum. Methods Phys. Res. B* **164** (2000) 241, https://doi.org/10.1016/S0168-583X(99)01086-1

20. C. D. Archubi, C. D. Denton, J. C. Eckardt, Angular dispersion of protons passing through thin metallic films, *Nucl. Instrum. Methods Phys. Res. B* **230** (2005) 53, https://doi.org/10.1016/j.nimb.2004.12.016

21. E. D. Cantero, G. H. Lantschner, N. R. Arista, Interaction of low energy protons, deuterons, H_2^+ and D_2^+ with carbon foils: energy-angle distributions and velocity dependence of the energy loss, *Eur. Phys. J. D* **65** (2011) 397, https://doi.org/10.1140/epjd/e2011-20397-3

22. C. Celedón, E. A. Sanchez, M. S. Moreno, Energy loss of protons and deuterons at low energies in Pd polycrystalline thin films, *Phys. Rev. A* **88** (2013) 012903, https://doi.org/10.1103/PhysRevA.88.012903

23. G. Amsel, G. Battistig, A. L'Hoir, Small angle multiple scattering of fast ions, physics, stochastic theory and numerical calculations, *Nucl. Instrum. Methods Phys. Res. B* **201** (2003) 325, https://doi.org/10.1016/S0168-583X(02)01740-8

24. J. E. Valdés, N. R. Arista, Energy-loss effects in multiple-scattering angular distributions of ions in matter, *Phys. Rev. A* **49** (1994) 2690, https://doi.org/10.1103/PhysRevA.49.2690

25. D. Schmaus, A. L'Hoir, Lateral and angular spread up to large energy losses for MeV protons transmitted through polyester films, *Nucl. Instrum. Methods Phys. Res. B* **4** (1984) 317, https://doi.org/10.1016/0168-583X(84)90575-5

26. E. Szilágyi, F. Pászti, G. Amsel, Theoretical approximations for depth resolution calculations in IBA methods, *Nucl. Instrum. Methods Phys. Res. B* **100** (1995) 103, https://doi.org/10.1016/0168-583X(95)00186-7

27. M. Mayer, Improved physics in SIMNRA 7, *Nucl. Instrum. Methods Phys. Res. B* **332** (2014) 176, https://doi.org/10.1016/j.nimb.2014.02.056

28. N. P. Barradas, K. Arstila, G. Battistig, M. Bianconi, N. Dytlewski, C. Jeynes, E. Kótai, G. Lulli, M. Mayer, E. Rauhala, E. Szilágyi, M. Thompson, International Atomic Energy Agency intercomparison of ion beam analysis software, *Nucl. Instrum. Methods Phys. Res. B* **262** (2007) 281, https://doi.org/10.1016/j.nimb.2007.05.018

29. M. Mayer, K. Arstila, K. Nordlund, E. Edelmann, J. Keinonen, Multiple scattering of MeV ions: Comparison between the analytical theory and Monte-Carlo and molecular dynamics simulations, *Nucl. Instrum. Methods Phys. Res. B* **249** (2006) 823, https://doi.org/10.1016/j.nimb.2006.03.148

30. E. G. Androulakaki, M. Kokkoris, M. Mayer, E. Mitsi, N. Patronis, E. Vagena, A comparative study of multiple scattering calculations implemented in general-purpose Monte Carlo and selected ion beam analysis codes, *Nucl. Instrum. Methods Phys. Res. B* **496** (2021) 71, https://doi.org/10.1016/j.nimb.2021.03.025

31. W. Möller, J. S. Williams, The lateral spread of MeV helium ions in carbon, aluminum, and copper, *Nucl. Instrum. Methods* **157** (1978) 205, https://doi.org/10.1016/0029-554X(78)90293-8

32. K. Khalal-Kouache, B. Aissous, A. Mekhtiche, A. C. Chami, Effect of energy loss in the simulation of slow ion scattering by a solid surface, *Nucl. Instrum. Methods Phys. Res. B* **266** (2008) 714, https://doi.org/10.1016/j.nimb.2007.11.043

33. A. Mekhtiche, K. Khalal-Kouache, Multiple scattering of low energy ions in matter: Influence of energy loss and interaction potential, *Nucl. Instrum. Methods Phys. Res. B* **354** (2015) 151, https://doi.org/10.1016/j.nimb.2014.11.086

34. A. Mekhtiche, K. Khalal-Kouache, Multiple scattering of low energy H^+ ions in matter: Approximation of mean energy on the Sigmund and Winterbon model, *Nucl. Instrum. Methods Phys. Res. B* **382** (2016) 32, https://doi.org/10.1016/j.nimb.2016.04.040

35. A. Mansour, A. Mekhtiche, K. Khalal-Kouache, Reflection of H^+ (2 keV) ions from metallic surfaces: transport theory calculation of the reflection probability with the mean energy approximation, *J. Surf. Invest.* **16** (2022) 1231, https://doi.org/10.1134/S1027451022060490

36. J. F. Ziegler, M. D. Ziegler, J. P. Biersack, SRIM – the stopping and range of ions in matter (2010), *Nucl. Instrum. Methods Phys. Res. B* **268** (2010) 1818, https://doi.org/10.1016/j.nimb.2010.02.091

37. G. de M. Azevedo, J. R. A. Kaschny, M. Behar, P. L. Grande, Ch. Klatt, S. Kalbitzer, Charge equilibration of He ions in the Si ⟨100⟩ channel, *Nucl. Instrum. Methods Phys. Res. B* **161–163** (2000) 96, https://doi.org/10.1016/S0168-583X(99)00677-1

38. P. Sigmund, Particle Penetration and Radiation Effects, Vol. 2: Penetration of Atomic and Molecular Ions (Springer, Cham, 2014), pp. 3–43, https://doi.org/10.1007/978-3-319-05564-0_1

39. J. C. Armstrong, J. V. Mullendore, W. R. Harris, J. B. Marion, Equilibrium charge-state fractions of 0.2 to 6.5 MeV helium ions in carbon, *Proc. Phys. Soc.* **86** (1965) 1283, `https://doi.org/10.1088/0370-1328/86/6/316`

40. G. Molière, Theorie der Streuung schneller geladener Teilchen I, *Z. Naturforsch. A* **2** (1947) 133, `https://doi.org/10.1515/zna-1947-0302`